Influence of the Cooling Conditions on the Temperature and Crystallinity Profiles Generated in a Sisal Fiber Reinforced-Polycaprolactone/Starch Molded Part

V. P. CYRAS[1], P. M. STEFANI[2], R. A. RUSECKAITE[1,3]*, *and* A. VÁZQUEZ[1]

[1]*Research Institute of Material Science and Technology*
INTEMA
Mar del Plata University
J. B. Justo 4302, 7600 Mar del Plata, Argentina

[2]*Facultad Regional Concepción del Uruguay*
Universidad Tecnológica Nacional
Ing. Pereira 676, 3260 Concepción del Uruguay, Argentina

[3]*Department of Chemistry*
Science Faculty
Mar del Plata University
Funes 3250, 7600 Mar del Plata, Argentina

In this work, we performed the simulation of the temperature and relative degree of crystallinity developed across the thickness of a sisal fiber reinforced-polycaprolactone/starch (30%SF-PCL/S) molded part under different cooling conditions. The non-isothermal kinetic model of Kamal and Chu (13) was used to predict the degree of crystallinity profiles. In order to obtain the temperature profiles, the energy equation was solved by treating the composite as a continuum using mass averaged physical properties. The results indicated that for cooling at a constant wall temperature, gradient-less crystallinity profiles for a wall temperature of 283 K and thicknesses lower than 10 mm are obtained. On the other hand, when cooling at a constant cooling rate, paired degree of crystallinity pieces can be obtained only for thicknesses lower than 2 mm. The continuum numerical approach used herein has the ability of predicting the optimal cooling cycle for manufacturing thick and crystallinity gradient-less SF-PCL/S parts. Polym. Compos. 25:461–469, 2004.

INTRODUCTION

Novel polymers and blends are being introduced in the market with the aim of fulfilling new environmental requirements concerning the effective management of post consumer waste (1). In recent years, the commercial introduction of blends based on starch and synthetic biodegradable polymers has opened new opportunities in this field. Particularly, polycaprolactone/starch blends (PCL/S) are receiving increasing industrial attention for use as commodity plastics. The PCL/S materials are attractive because of their biodegradability. Also, they allow the possibility of using the same transformation technologies applied to traditional plastics (2, 3). However, the current price of such materials limits their use to a few exclusive applications. One economically and ecologically attractive approach to overcoming these limitations is to incorporate natural fibers into biodegradable polymers. In this way, it is possible to obtain environmentally friendly composite materials called *biocomposites* that are quite similar to the already known synthetic fiber reinforced plastics (4).

Processing of semicrystalline polymeric composites is usually performed under non-isothermal conditions. During fabrication, a polymeric material is exposed to one or more cycles of heating, melting, cooling and solidification, which ultimately determine the morphology

*To whom correspondence should be addressed. E-mail: roxana@fi.mdp.edu.ar

Published online in Wiley InterScience (www.interscience.wiley.com).
DOI: 10.1002/pc.20039

and final properties of the product (5). Further, cooling a thick part too rapidly produces temperature gradients through the thickness, which may subsequently lead to crystallinity and morphology gradients.

Many biodegradable polymers, such as polyhydroxyalcanoates (PHAs), polycaprolactone (PCL), thermoplastic starch (TPS), and Mater Bi™, have been tested in order to be used as matrix materials for the fabrication of biocomposites (1, 4, 6–10). In addition to an expected improvement in mechanical properties, some studies have shown that the incorporation of reinforcing natural short fibers can significantly influence the crystallization rate and crystalline morphologies. In thermoplastic matrix composites, short fibers can act as nucleating agents. In isotatic polypropylene (iPP), the presence of synthetic or natural fiber produces a dramatic decrease of the half-time of crystallization, as well as an increase in the overall crystallization rate for all the fibers analyzed, including sisal fiber (11). The same effect was found for wood fibers on the crystallization of polyhydroxybutyrate-co-hydroxyvalerate (PHB-co-HV). The strong effect of the fibers on the crystallization rate is presumed to be due to the increase of the heterogeneous nucleation on the fiber surface (5). On the other hand, Cyras *et al.* (9) have analyzed the crystallization kinetics in isothermal conditions for polycaprolactone/starch blends (PCL/S) and their reinforced sisal fiber composites (SF-PCL/S), with 5 to 30 wt% of sisal fiber content. Induction times (t_i) for the composites were higher than those obtained for PCL/S neat matrix. However, half-time crystallization ($\tau_{1/2}$) values were almost not affected by the presence of sisal fibers. Thus, sisal fiber does not act as a nucleating agent for a PCL/S matrix. It is evident that, in order to process biodegradable matrix composite with tailored final properties, the crystallization behavior under non-isothermal conditions and in the presence of fibers must be understood.

In our previous work, we modeled the temperature and relative degree of crystallinity profiles generated during the non-isothermal cooling step of a PCL/S blend (12). In the present work, we present the evolution of temperature and relative degree of crystallinity profiles developed through the thickness of a part of polycaprolactone/starch matrix reinforced with 30% sisal fiber (SF), as a function of cooling conditions. The composite is treated as a continuum, i.e., the physical properties of the fiber and the matrix are mass-averaged. Differential Scanning Calorimetry (DSC) is used to determine the experimental degree of crystallinity under non-isothermal conditions. Experimental data are correlated by using the Kamal and Chu model (13).

EXPERIMENTAL

Materials and Methods

A commercial blend based on polycaprolactone (PCL) and starch (S) was provided by Novamont (Italy). Starch and natural additive content are higher than 40 wt% (3). Sisal fiber (SF), used as the reinforcing material, was supplied by Brascorda (Brazil). The PCL/S blend was reinforced with 30 wt% of sisal fiber (30%SF-PCL/S). The average fiber diameter (D) and length (L) were determined by optical microscopy of fibers extracted with an organic solvent from the matrix (9). The average length/diameter ratio (L/D) was 17.3. A twin-screw extruder (Haake Rheomex CTW 100) was used to disperse the fibers in the polymeric matrix using the same conditions as those reported elsewhere (9).

The non-isothermal melt crystallization kinetics was analyzed by calorimetric analysis by using a Mettler 30 Differential Scanning Calorimeter (DSC), operating from −50°C to +350°C under a nitrogen atmosphere. Samples at room temperature were heated to 80°C, at a heating rate of 10°C/min. The samples were kept at 80°C for 10 min, and then were subsequently cooled to −50°C using different scanning rates (0.083, 0.25 and 0.5 K/s).

The exothermic crystallization peaks obtained for different cooling conditions can be integrated to compute the relative degree of crystallinity, *Xr*. Assuming that the crystallization enthalpy is directly related to the quantity of crystallized polymer, the relative degree of crystallinity as a function of the crystallization temperature (T) was obtained as:

$$Xr = \frac{\int_{T_0}^{T} \left(\frac{dH_c}{dT}\right) dT}{\int_{T_0}^{T_\infty} \left(\frac{dH_c}{dT}\right) dT} \quad (1)$$

where ΔH_c is the differential crystallization enthalpy; T is the crystallization temperature and T_0 and T_∞ represent the onset and the end of the crystallization peak, respectively. Since the experimental crystallization enthalpies were slightly affected by the cooling conditions (18,430, 19,080 and 25,440 J/kg for 0.083, 0.25 and 0.5 K/s, respectively), an average value of ΔH_c was taken (*Table 1*).

Non-Isothermal Kinetic Model

Overall isothermal crystallization of semicrystalline polymers is mainly described by the Avrami macrokinetic approach, according to the following equation (14):

$$Xr\,(t) = 1 - \exp\,(-k\,t'') \quad (2)$$

Table 1. Physical Constants Used in the Simulation.

Physical Constant	Values	
Thermal conductivity, k_c	0.1348	J/s.m.K
Specific heat, *Cp*	1301.7	J/K.kg
Density, ρ	1286.9	kg/m^3
Crystallization heat, ΔH_c	20,671	J/kg
Equilibrium melting temperature, T_m^0	338	K
Initial temperature, T_0	353	K
Activation energy non-isothermal crystallization, *Ea*	1115	J/mol
Kinetic exponent, *n*	2.29	
Pre-exponential constant, *k*	0.0386	s^{-n}
Activation energy isothermal induction time, E_i	2600	J/mol
Pre-exponential constant isothermal induction time, k_{io}	1.6×10^{-4}	1/s

where Xr is the relative degree of crystallinity, t is time and n and k values are related to the mechanism of crystallization.

Non-isothermal crystallization processes have been traditionally represented by integral or differential expressions derived from the classical Avrami equation with a temperature dependent kinetic constant (13–16). Differential expressions are more suitable for modeling purposes and can be easily related to calorimetric data. The integral model of Kamal and Chu (13) is expressed in its differential form by Lin (17) as:

$$\frac{dXr}{dt} = n\,k(T)(1 - Xr)t^{n-1} \tag{3}$$

This model can be reduced to the classical Avrami expression (*Eq 2*) for isothermal conditions.

For modeling purposes, the induction time must be considered. The induction time is associated with the delay before the onset of massive nucleation (18). Heterogeneous nucleation is a thermally activated phenomenon, and its effects can be macroscopically detected by isothermal DSC experiments. The exothermic signal can be observed only after a delay, namely the induction time, attributed to the formation of nuclei of critical size (19). The temperature dependence of the induction time (t_i) can be described by (14):

$$t_i = k_{i0} \exp\left[\frac{E_{i2}}{R(T_g - T)}\right]\exp\left[\frac{E_{i1}}{R(T_m^0 - T)}\right] \tag{4}$$

where k_{i0} is the pre-exponential factor. The two exponential terms account for the driving force of the nucleation above the glass transition temperature (T_g) and below the theoretical melting point (T_m^0); E_{i1} and E_{i2} are the activation energies for these contributions. For PCL/starch blends, the T_g corresponds to that of the PCL (T_g PCL = −60°C). The first term in *Eq 4* can be neglected because cooling temperatures are not lower than room temperature. So, *Eq 4* is simplified as follows:

$$t_i = k_{i0} \exp\left[\frac{E_i}{R(T_m^0 - T)}\right] \tag{5}$$

The induction time plays a fundamental role in determining the onset time for the crystal growth, and it is a relevant parameter from a processing point of view. Klein *et al.* (18) have analyzed the effect of nucleating agents or fibers on the induction time. Their results show that the presence of nucleating agents shortens the induction time, because the nucleation does not depend on the formation of a seed by the polymer, and favors the crystallization kinetics. Nucleating agents are usually added to polymers in order to accelerate the overall crystallization process. In polymer composites, nucleation on a synthetic fiber surface has been reported for nylon 66 (18), poly(etherketone) (20) and polypropylene (11, 21, 22). However, induction time cannot be determined experimentally in non-isothermal conditions. The non-isothermal induction time (t_{ni}) is computed by using a dimensionless parameter $\mathcal{Q}$:

$$\mathcal{Q} = \int_0^{t_{ni}} \frac{dt^*}{t_i} \tag{6}$$

where t_i is the isothermal induction time given by *Eq 5*. Numerical integration of *Eq 6* is performed taking $t^* = 0$ at the melting temperature (T_m^0). The value $t^* = t_{ni}$ at which $\mathcal{Q}$ reaches the unity represents the non-isothermal induction time (19).

The kinetic constant in *Eq 3* depends on temperature as described by the following equation (19):

$$k = k_0 \exp\left[\frac{-Ea_2}{R(T_g - T)}\right]\exp\left[\frac{-Ea_1}{R(T_m^0 - T)}\right] \tag{7}$$

where k_0 is a pre-exponential factor. The first exponential accounts for the factors above T_g which induces the cold crystallization, while the second exponential term accounts for the driving force of crystallization given by the degree of undercooling, $(T_m^0 - T)$. As mentioned before, the first exponential can be neglected for PCL/S blends. So, *Eq 7* can be written as:

$$k = k_0 \exp\left[\frac{-Ea}{R(T_m^0 - T)}\right] \tag{8}$$

where Ea is the crystallization activation energy, k_0 is the pre-exponential constant, T_m^0 is the theoretical melting temperature and R is the gas constant.

A non-linear regression method based on Marquardt algorithm (23) was used to find the best fitting parameters to the differential form of Kamal and Chu equation (*Eqs 3–8*). The theoretical melting temperature (T_m^0), activation energy for the induction (E_i) and pre-exponential factor for the induction time (k_{0i}) were taken from the literature (9) and are summarized in *Table 1*.

Model Equations

A two-parallel-plate mold was used for the simulation of the solidification process. This geometry allows for one-dimensional flow (*Fig. 1*). The one-dimensional unsteady-state heat transfer rate through the mold thickness is given by the following energy equation:

$$\rho\,Cp\,\frac{\partial T}{\partial t} = k_c\,\frac{\partial^2 T}{\partial y^2} + \rho(-\Delta H_c)\,\frac{dXr}{dt} \tag{9}$$

This equation relates the relative degree of crystallinity (Xr) and temperature (T), as a function of time (t) and the position in the mold thickness (y) for given values of crystallization heat (ΔH_c), thermal conductivity (k_c), density (ρ) and specific heat (Cp). The first term on the right-hand side in *Eq 9* represents the heat transfer due to conduction, and the second represents the heat source associated with the heat generated during crystallization (*Eq* 3). The thermal conductivity, the density and the specific heat were assumed to be constant with temperature. This assumption is valid in the temperature range used in the present study.

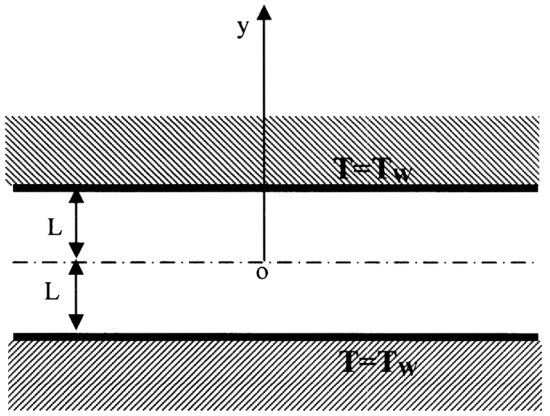

Fig. 1. Configuration of the mold used for the simulation of the solidification process.

Equation 9 can be written as:

$$\frac{\partial T}{\partial t} = \alpha \frac{\partial^2 T}{\partial y^2} + \frac{(-\Delta H_c)}{Cp} \frac{dXr}{dt} \quad (10)$$

where $\alpha = k_c/\rho\ Cp$ is the thermal diffusivity.

The dimensionless form of the energy equation (*Eq10*) may be written as:

$$\frac{\partial \theta}{\partial \lambda} = \frac{\partial^2 \theta}{\partial \xi^2} + \beta \frac{dXr}{d\lambda} \quad (11)$$

where

$$\theta = T/T_0 \quad \lambda = t\alpha/L^2 \quad \xi = y/L \quad \beta = \Delta H_c/Cp\ To \quad (12)$$

The density of 30%SF-PCL/S composites was calculated as a mixture rule:

$$\rho = V_{PCL}\,\rho_{PCL} + V_{starch}\,\rho_{starch} + V_{sisal\ fiber}\,\rho_{sisal\ fiber} \quad (13)$$

where ρ_{PCL}, ρ_{starch} and $\rho_{sisal\ fiber}$ represent the density of the PCL, starch and sisal fiber, respectively (24–26), and V_{PCL}, V_{starch} and $V_{sisal\ fiber}$ are the volume fraction content of each component in the composite.

The thermal conductivity was calculated combining the thermal conductivities of the three components, using the parallel model and the corresponding volume fraction of each one:

$$\frac{1}{k_c} = \frac{V_{PCL}}{k_{PCL}} + \frac{V_{starch}}{k_{starch}} + \frac{V_{sisal\ fiber}}{k_{sisal\ fiber}} \quad (14)$$

where k_{PCL}, k_{starch} and $k_{sisal\ fiber}$ are the individual thermal conductivities taken from the literature (24, 27, 28).

The specific heat capacity was calculated as:

$$Cp = w_{PCL}\,Cp_{PCL} + w_{starch}\,Cp_{starch} + w_{starch}\,Cp_{starch} \quad (15)$$

where Cp_{PCL}, Cp_{starch} and $Cp_{sisal\ fiber}$ are the heat capacities of the individual components (24, 25, 28), w_{PCL}, w_{starch} and $w_{sisal\ fiber}$ are the weight fraction content of PCL, starch and sisal fiber, respectively. *Table 1* shows the parameters used in the dimensionless energy equation.

The boundary conditions are the following:

- For cooling under a constant cooling rate:

$$y = 0 \quad dT/dy = 0 \quad (16)$$

$$y = L \quad T = T_w(t) = To + qt \quad (17)$$

where q is the cooling rate and To is the initial temperature.

- For cooling under a constant wall temperature (T_w):

$$y = 0 \quad dT/dy = 0 \quad (18)$$

$$y = L \quad T = T_w \quad (19)$$

The initial conditions are:

$$T = To,\ Xr = 0\ at\ t = 0\ \forall\ y \quad (20)$$

RESULTS AND DISCUSSION

Modeling of the Non-Isothermal Crystallization Kinetics

The effect of different cooling rates on the non-isothermal melt crystallization of 30%SF-PCL/S has been studied by DSC. *Figure 2* represents the crystallization thermograms obtained for 30%SF-PCL/S at different cooling rates (0.083, 0.25 and 0.5 K/s). The exothermic peak temperature (*Tp*), relative degree of crystallinity at *Tp*, (X_{rTp}) and the half-time ($\tau_{1/2}$), are summarized in *Table 2*. For comparison purposes, the values of the unfilled matrix PCL/S are also included. The X_{rTp} and *Tp* values are very close for both systems. The analysis of *Table 2*, suggests that fiber reinforcement slightly increases the overall crystallization rate, given by the lower half-time values. The relative degree of crystallinity is not significantly affected by fiber reinforcement. The variations observed in the relative degree of crystallinity can be related to two different experimental factors: the uncertainty in heat flow measurements and the inaccuracy in the fiber content of the specimen analyzed by calorimetry (6).

Integration of the exothermic peaks gives the relative degree of crystallinity as a function of temperature (*Eq 1*). In order to obtain kinetic information, the

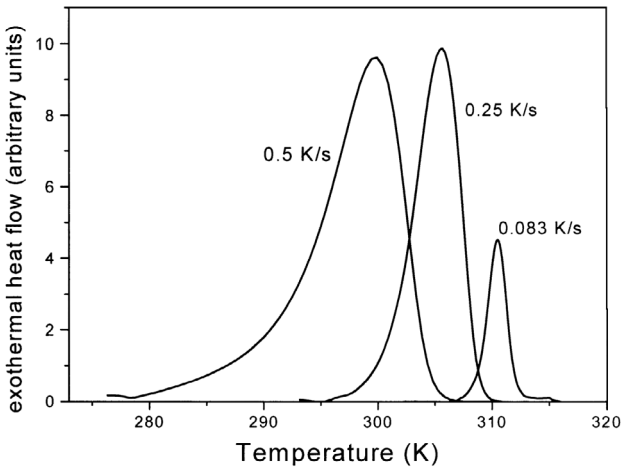

Fig. 2. Crystallization curves obtained at different cooling rates.

Table 2. Peak Temperature (*Tp*), Relative Degree of Crystallinity at *Tp* (X_{rTP}) and Crystallization Half-Times ($\tau_{1/2}$) for the Melt Crystallization of PCL/S and 30%SF-PCL/S.

Cooling Rate (K/s)	30%SF-PCL/S			PCL/S		
	T_p	X_{rTP}	$\tau_{1/2}$ (min)	T_p (K)	X_{rTP}	$\tau_{1/2}$ (min)
0.083	311	0.43	36	310	0.48	39.7
0.25	305	0.34	33	304	0.44	35
0.5	299	0.31	27	302	0.33	32.4

experimental relative degree of crystallinity data collected over a wide range of cooling rates, were fitted with the Kamal and Chu differential model (13, 17). A nonlinear multivariable regression analysis based on Marquard method (23) was used. Cyras *et al.* (9) described the 30%SF-PCL/S crystallization process by applying the integral expression of Nakamura (15), which extends the general Avrami theory to non-isothermal conditions, using the kinetic parameters derived from the isothermal analysis. It must be taken into account that in non-isothermal conditions, the kinetic parameters do not have the same physical significance as in isothermal experiments. This is because in non-isothermal conditions, temperature changes constantly. The multivariable approach used in the present work directly fits the experimental data to the Kamal and Chu macrokinetic model. In a nonlinear regression method, the best N number of parameters are searched in order to find the global minimum in the sum of the squares errors (29). Thus, the kinetic parameters are provided automatically by the program with the best fit. *Figure 3* shows the comparison between experimental and predicted data. It can be seen that the curves are horizontally shifted in temperature, as a result of a rate-dependent induction time preceding the onset of the crystallization (18). The model represents experimental data in a broad range of *Xr* values and shows a good performance, specially at low cooling rates. The predicted kinetic parameters were: activation energy *Ea* = 1155 J/mol; the pre-exponential factor k_0 = 0.0386 s^{-n}, and the Avrami exponent n = 2.29. In a previous work, we determined the kinetic parameters for the unfilled matrix by using the same analytical procedure (12). The predicted activation energy was 1954 J/mol and the pre-exponential constant was 0.85058 s^{-n}. By comparison of both *Ea* values, it is easy to conclude that the activation energy for the composite is lower than that of the unfilled matrix. So, the presence of sisal fiber seems to increase the overall crystallization rate. This is in agreement with the lower crystallization half-times experimentally obtained for the reinforced matrix (*Table 2*).

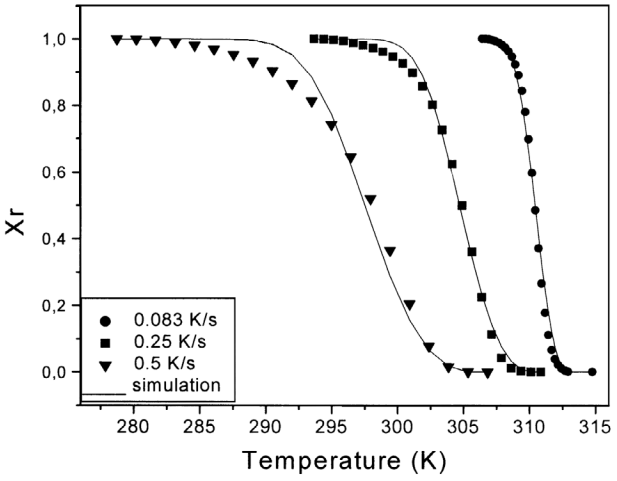

Fig. 3. Comparison between experimental and predicted crystallinity data at different cooling rates. Solid lines correspond to the model predictions and points are experimental data.

The analytical procedure used in this work allows us to obtain a single set of kinetic parameters for a wide range of cooling rates. These data can be used in modeling actual processing conditions.

Temperature and Crystallinity Gradients Generated Under Cooling at Constant Wall Temperature

The effective cooling is normally achieved by using a constant cooling temperature or a constant cooling rate, applied to the mold wall. In ejection molding, the rate of cooling is the main parameter in determining the production rate and the final properties of the end products. The optimal cooling conditions are those that allow one to obtain uniform temperature across the thickness of the part in a short molding time (30).

The temperature, crystallization rate and relative degree of crystallinity unsteady-state profiles developed during cooling under different temperatures applied to the mold wall for a 30%SF-PCL/starch. They were calculated from temperature and crystallinity variations with time (*Eq 10*) with the non-isothermal crystallization model (*Eqs 3–8*). An implicit finite-difference method (Crank-Nicholson scheme) was used to solve the energy equation. The dX_r/dt in the heat source term of *Eq 10* was evaluated by using an explicit method. The sample thickness (from 1 to 10 mm) was divided into 10 evenly spaced nodes between the centerline and the wall (*Fig. 1*). The time step at which the system was solved was less than 0.002 s. The wall temperatures were 293, 303 and 313 K, which are in the range of the usual cooling temperatures for most of thermoplastics (30).

In the cooling process, three different steps can be distinguished:

1) Cooling of the piece from the molten state, before the beginning of crystallization. In this stage, the

temperature profiles respond to Fourier's law under non-steady conditions, which is a function of the conductivity of the melt, the thickness of the part and the cooling conditions.

2) Cooling during crystallization. The temperature profiles generated are the result of two competing factors: (a) the rate of heat generated by the exothermic crystallization reaction and (b) the conductive heat flux towards the walls. As the crystallization begins, an increment in temperature occurs in the center of the sample.

3) Cooling a solid. After crystallization, the temperature profiles are controlled by Fourier's law. In this stage, they are a function of the conductivity of the solid.

The temperature profiles may lead to crystallinity and morphology gradients that produce undesirable variations in the mechanical properties of the part. Therefore, the model was used to predict the effect of cooling rate and thickness of the part on temperature, crystallization rate and crystallinity evolution during the cooling step.

The effect of the cooling temperature (313 K) on the temperature profiles as a function of time for different positions along the *y*-axis, is shown in *Fig. 4*. The distance between two consecutive sampling points is 0.2 mm. The slope of each temperature curve in *Fig. 4* represents the local cooling rate as a function of time for the different nodes within the part. Near the wall, the cooling rate was relatively faster compared to that at the center of the part. As the wall temperature increases (*Fig. 5*), the local cooling rate decreases from the wall to the center, where an increment was observed. This increment is associated with the crystallization process, during which the heat is released. This exothermic process produces an increment in the local crystallization temperatures (or a decrease in the crystallization rates), being more pronounced in the center.

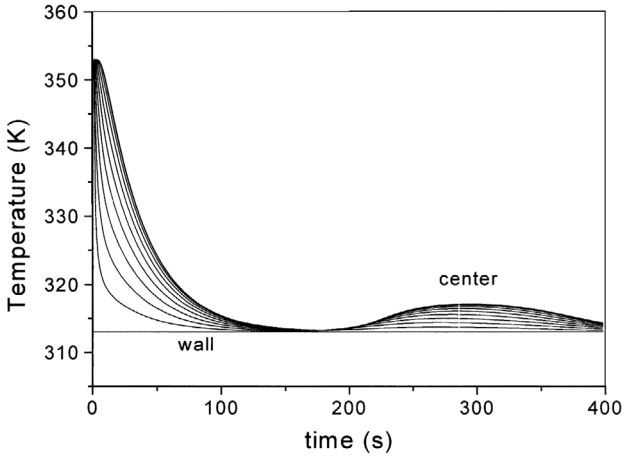

Fig. 4. Cooling curves for different positions along the horizontal axis of a 30%SF-PCL/S part of thickness 2 mm, cooled at 313 K.

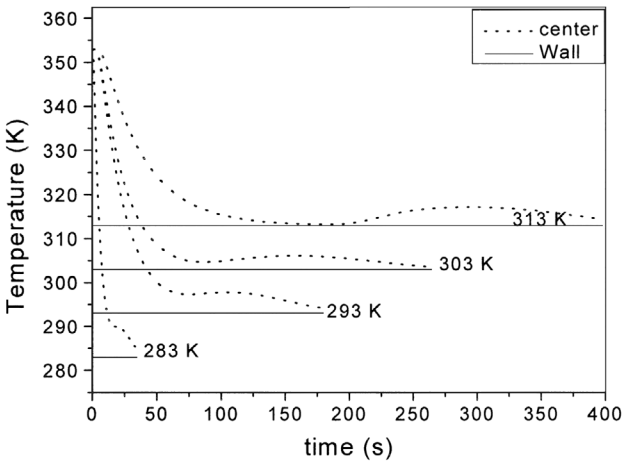

Fig. 5. Effect of the cooling temperature on the temperature profiles at the center of a 4-mm-thick part.

As expected, the higher the cooling temperature, the lower the crystallization rate.

The same behavior is observed as the thickness of the part increases, as shown in *Fig. 6*. The predicted temperature and crystallization rate profiles for two specific positions, the wall and the center, generated under a cooling temperature of 293 K for thicknesses of 2 and 10 mm, are represented in *Figs. 7* and *8*, respectively. For the 2-mm-thick part, the crystallization at the wall begins as soon as the cooling process starts. This is due to the high driving force given by the temperature difference between the polymer melt and the cooling temperature. No exothermic peak is observed as a consequence of the boundary condition imposed. In the core region, the crystallization rate has a maximum at 24.8 s. The model predicts paired relative degree of crystallinity gradients achieved in about 45 s. On the other hand, for the 10-mm-thick part, the model predicts well-defined surface-to-center crystallinity. The maximum crystallization rate at the wall occurred at

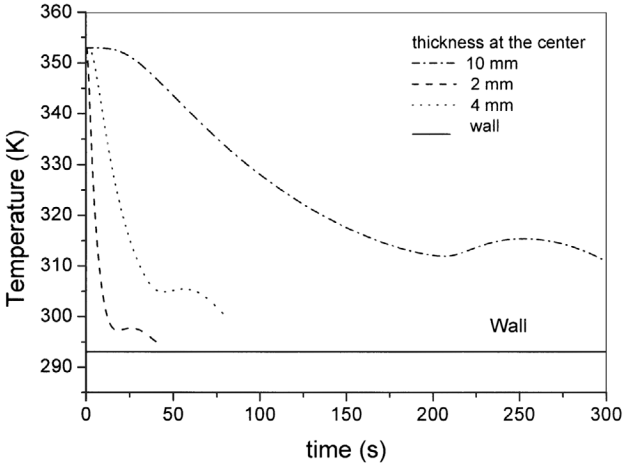

Fig. 6. Effect of the sample thickness on the temperature profiles generated in a 30%SF-PCL/S part cooled at 293 K: (___) wall and center (----) of the part.

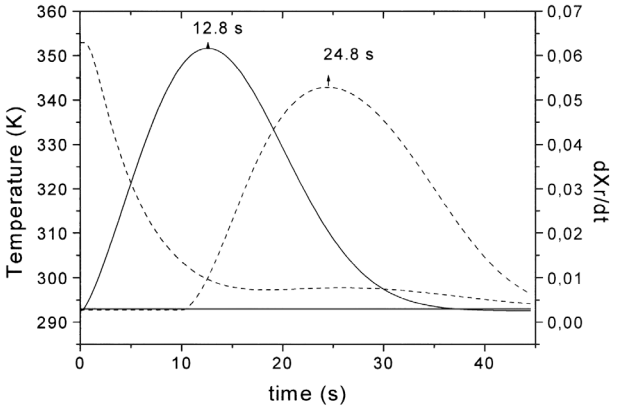

Fig. 7. Predicted crystallization rate and temperature gradients for two specific positions, the wall (___) and the center (----), generated under a cooling temperature of 293 K for a 30%SF-PCL/S 2-mm-thick part.

20 s, whereas at the core region, a period of about 300 s was needed to complete the crystallization (*Fig. 8*). The shoulder observed in the crystallization rate curve corresponding to the core region is associated with the increase in the local temperature during cooling. This increment produces a delay in the crystallization, and impaired crystallinity profiles are predicted. These results suggest that the influence of the conduction term is major, as the thickness or the wall temperature increases. As a result, the higher the cooling temperature (or the thickness), the lower the crystallization rate. As expected, by decreasing the cooling temperature with an appropriate chilling fluid, almost uniform crystallinity profiles may be reached in a relatively short time, even for thicknesses of about 10 mm.

Temperature and Crystallinity Gradients Generated Under Cooling at Constant Cooling Rate

The model was also used to predict the temperature and relative degree of crystallinity profiles generated during the solidification step of a part of 30%SF-PCL/S under different cooling rates. The cooling rates used in the simulation were in the range of 0.083 to 0.5 K/s and were similar to those reported in the literature for studying the non-isothermal crystallization process of thermoplastic matrix composites (11, 12, 21, 31).

The effect of the cooling rate on the temperature profile generated within a 4-mm-thick part is shown in *Fig. 9*. As the cooling rate increases, the surface-to-center temperature gradients are more significant. These temperature gradients may lead to variations in crystallinity across the part. In order to reproduce actual processing conditions, the total cycle time was determined as the time taken for the first node of the polymer melt (next to the mold wall), to reach the room temperature (Tr = 293 K). Predicted temperature and crystallinity gradients for a 10-mm-thick part cooled at two extreme cooling rates, 0.5 and 0.083 K/s, are shown in *Figs. 10a* and *10b*, respectively. For a cooling rate of 0.083 K/s, the wall reaches room temperature at about 705 s. The simulation obtained by using the crystallization kinetics coupled with the energy equation predicts almost complete crystallization across the thickness, except for the inner part. On the other hand, for 0.5 K/s, the wall reaches room temperature in about 120 s, and only the wall and a few layers of polymer next to it can crystallize, and no crystallization in the inner part is reached. However, for a 2-mm-thick part, the model predicts complete crystallization from the wall to the center, for all practical purposes, under all the cooling rates analyzed (*Fig. 11*). So, the surface-to-center crystallinity gradients become more significant as either the thickness or the cooling rate increases. Cooling at a constant cooling rate may be applied only to pieces with thicknesses lower than 2 mm. In order to manufacture thick parts in actual processing conditions, the optimal cycle should be: to cool the sample at a high constant cooling rate (i.e., 0.5 K/s) up to room temperature, and then to maintain the part at constant temperature (i.e., room temperature) until complete crystallization.

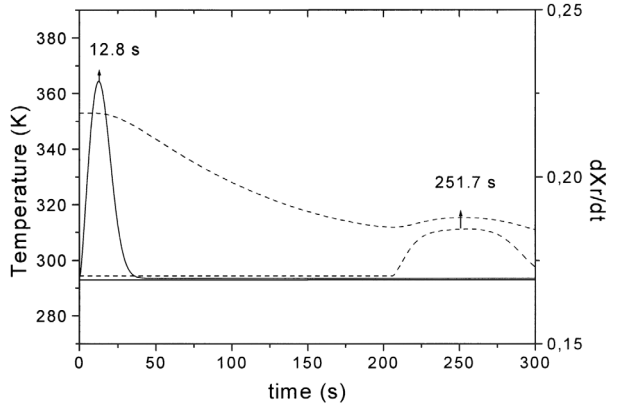

Fig. 8. Predicted crystallization rate and temperature gradients for two specific positions, the wall (___) and the center (---), generated under a cooling temperature of 293 K for a 30%SF-PCL/S 10-mm-thick part.

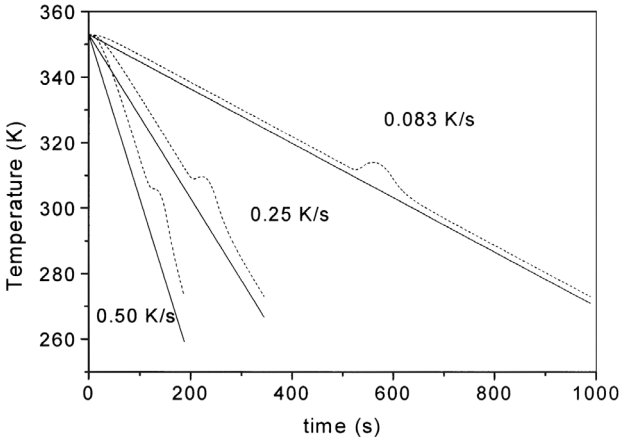

Fig. 9. Effect of the different cooling rates on the temperature variation at the wall (___) and at the center (----) for a 30%SF-PCL/S 4-mm-thick part.

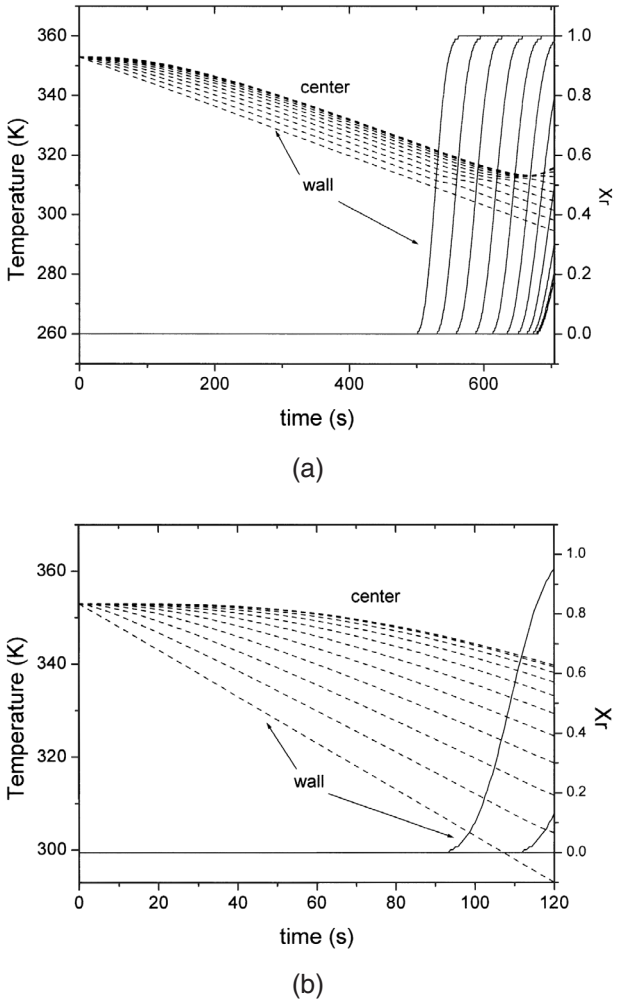

Fig. 10. Temperature (__) and crystallinity gradients (---) generated in a 10-mm-thick part of 30%SF-PCL/S cooling at two extreme cooling rates: a) 0.083 K/s; b) 0.5 K/s.

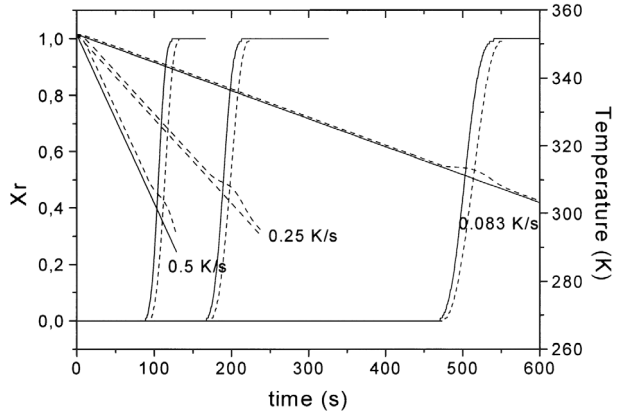

Fig. 11. Temperature and crystallinity gradients generated within a 2-mm-thick part of 30%SF-PCL/S cooling at three different temperatures (0.5, 0.25 and 0.083 K/min) for two positions, the wall (___) and the center (---).

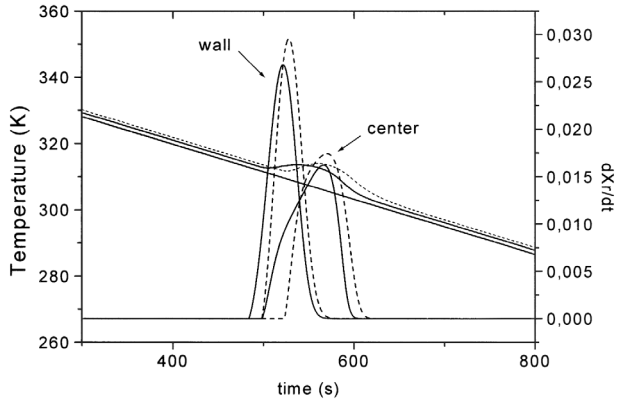

Fig. 12. Comparison of the simulated crystallization rates and temperature variation of PLC/S (___) and 30%SF-PCL/S (---) as a function of the time and for two specific positions, the wall and the center.

The effect of fibers on the cooling process was also analyzed. *Figure 12* shows the crystallization rate and temperature variations for PCL/S (solid lines) and 30%SF-PCL/S (dashed lines) at the wall and in the inner part of samples of 4 mm, cooled under the same conditions (0.083 K/s). The effect of the thermal conductivity in the crystallization process is quite relevant. The PCL/S crystallization is faster even in the core region because the heat generated by the exothermic crystallization reaction in the composite is higher than the conductive heat flux. This exothermic process increases the local temperature, with the subsequent delay in the crystallization. However, once the crystallization begins, the process at each position (wall and center) becomes faster for the composite than for the unfilled matrix, for all the cooling rates and thicknesses analyzed. This result is expected from of the lower activation energy value predicted for the composite.

CONCLUSIONS

The numerical simulation developed in this work was able to predict the temperature, relative degree of crystallinity and crystallization rate profiles developed during the cooling stage of a sisal fiber-reinforced polycaprolactone/starch matrix as a function of the non-isothermal cooling conditions. The continuum numerical approach used herein has the ability of predicting, in a single step, the optimal cooling conditions for obtaining paired relative degree of crystallinity profiles. For cooling at a constant wall temperature, the model predicts paired crystallinity profiles for a wall temperature of 283 K and thicknesses lower than 10 mm. On the other hand, cooling at a constant cooling rate may be applied only to pieces with thicknesses lower than 2 mm. In order to manufacture thick and gradient-less SF-PCL/S pieces, the optimal cooling cycle should be: to cool at higher constant cooling rate up to room temperature, and then to maintain the part at room temperature up to complete crystallization.

ACKNOWLEDGMENTS

Financial support from the National Research Council (CONCET, Argentina) is gratefully acknowledged. The authors would like to thank Dr. P. Haure for her useful advice.

REFERENCES

1. P. Gatenholm, J. Kubat, and A. Mathiasson, *J. Appl. Polym. Sci.*, **42**, 1667 (1992).
2. C. Bastioli, V. Bellotti, A. Montino, G. Tredici, R. Lombi, and R. Ponti, United States Patent 5,412,005 (1995).
3. C. Bastioli, V. Bellotti, L. Del Giudice, and G. Gilli, in *Biodegradable Polymers and Plastics,* M. Vert, J. Feijen, A-C. Albertsson, G. Scott, and E. Chiellini, eds., Royal Society of Chemistry, Cambridge, U.K. (1992).
4. A. K. Mohanty, M. Misra, and G. Hinrichsen, *Macromol. Mater. Eng.*, **276/277**, 1 (2001).
5. J. M. Kenny and A. Maffezzoli, *Polym. Eng. Sci.*, **31**, 607 (1991).
6. V. E. Reinsch and S. S. Kelley, *J. Appl. Polym. Sci.*, **64**, 1785 (1997).
7. H. Nitz, H. Semke, R. Landers, and R. Mülhaupt, *J. Appl. Polym. Sci.*, **82**, 1972 (2001).
8. M. Neus Anges and A. Dufresne, *Macromolecules*, **33**, 8344 (2000).
9. V. P. Cyras, J. M. Kenny, and A. Vázquez, *Polym. Eng. Sci.*, **41**, 1521 (2001).
10. V. P. Cyras, J. Martucci, S. Iannace, and A. Vázquez, *Journal of Thermoplastic Composite Materials*, **15**, 253 (2002).
11. M. A. Lopez Manchado, J. Biaggiotti, L. Torre, and J. M. Kenny, *Polym. Eng. Sci.*, **40**, 2194 (2000).
12. R. A. Ruseckaite, P. M. Stefani, V. P. Cyras, J. M. Kenny, and A. Vázquez, *J. Appl. Polym. Sci.*, **82**, 3275 (2001).
13. M. R. Kamal and E. Chu, *Polym. Eng. Sci.*, **23**, 27 (1983).
14. B. Wunderlich, *Macromolecular Physics*, Vol. 2, Academic Press, New York (1977).
15. K. Nakamura, K. Katayama, and T. Amano, *J. Appl. Polym. Sci.*, **17**, 1031 (1973).
16. T. Ozawa, *Polymer*, **12**, 150 (1971).
17. C. C. Lin, *Polym. Eng. Sci.*, **23**, 113 (1983).
18. N. Klein, D. Selevansky, and G. Marom, *Polymer Composites*, **16**, 189 (1995).
19. L. Torre, A. Maffezzoli, and J. M. Kenny, *J. Appl. Polym. Sci.*, **56**, 985 (1995).
20. Y. Lee and R. Porter, *Polym. Eng. Sci.*, **26**, 633 (1986).
21. A. K. Gupta, V. P. Gupta, R. H. Peters, W. G. Harland, and J. P. Berry, *J. Polym. Sci. Polym. Phys.*, **27**, 4669 (1982).
22. H-J. Tai, W-Y. Chiu, L-W. Chen, and L. Chu, *J. Appl. Polym. Sci.*, **42**, 3111 (1991).
23. W. Marquardt, *SIAM J.*, **11**, 431 (1963).
24. Y. Agari and A. Ueda, *J. Polym. Sci. Polym. Phys.*, **32**, 56 (1994).
25. D. Helman and D. Lund, eds., *Handbook of Food Engineering*, Marcel Dekker, New York (1992).
26. A. Paul and S. Thomas, *J. Appl. Polym. Sci.*, **63**, 247 (1997).
27. J. Brandrup and E. Immergut, eds., *Polymer Handbook,* 2nd ed., Wiley, New York (1975).
28. S. Rahman, ed., *Food Properties Handbook*, CRC Press, Boca Raton, Fla. (1995).
29. R. M. Patel and J. E. Spruiell, *Polym. Eng. Sci.*, **31**, 730 (1991).
30. N. Sombatsompop and A. Tangsongcharoen, *J. Appl. Polym. Sci.*, **82**, 2087 (2001).
31. C. N. Velisaris and J. C. Seferis, *Polym. Eng. Sci.*, **28**, 583 (1988).